cSINGV v1.0: Development and evaluation of a 1.5 km coupled atmosphere-ocean-wave modelling system for the Western Maritime Continent

Supplementary Material

This supplement provides additional figures and tables supporting the evaluation of the ocean and wave components, precipitation diagnostics, case studies, and air–sea flux analysis presented in the main manuscript.

S1. Model domain and analysis regions

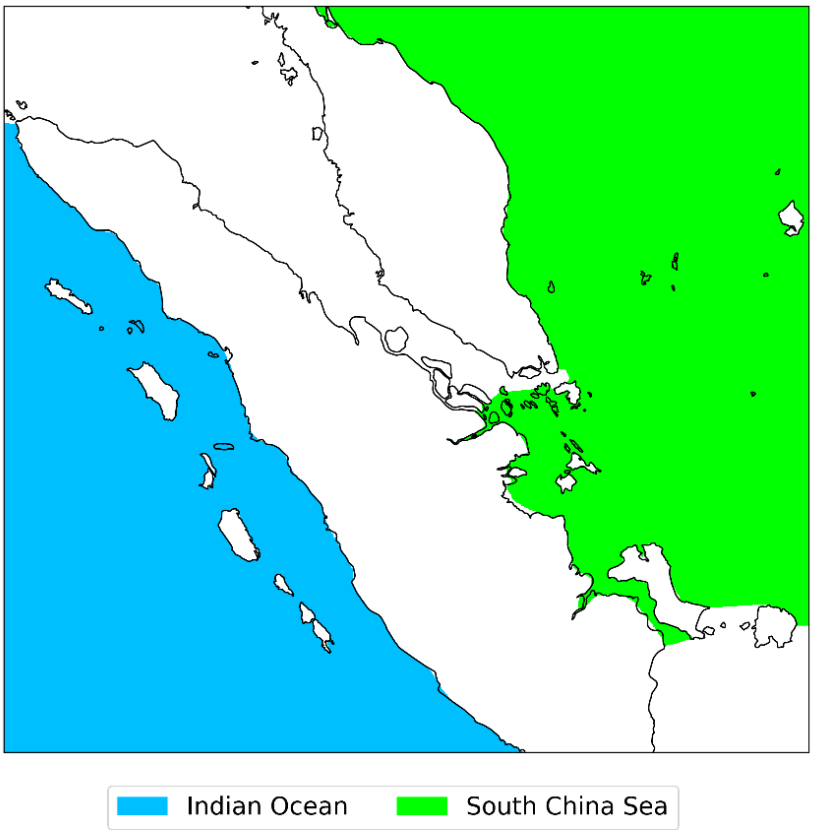

Figure S1. Model domain of the coupled atmosphere–ocean–wave system. Shaded regions indicate the subdomains used for ocean evaluation: the Indian Ocean (blue) and the South China Sea (green). These regions represent contrasting dynamical regimes used for regional analysis in Section 4.1.

S2. Ocean model additional evaluation

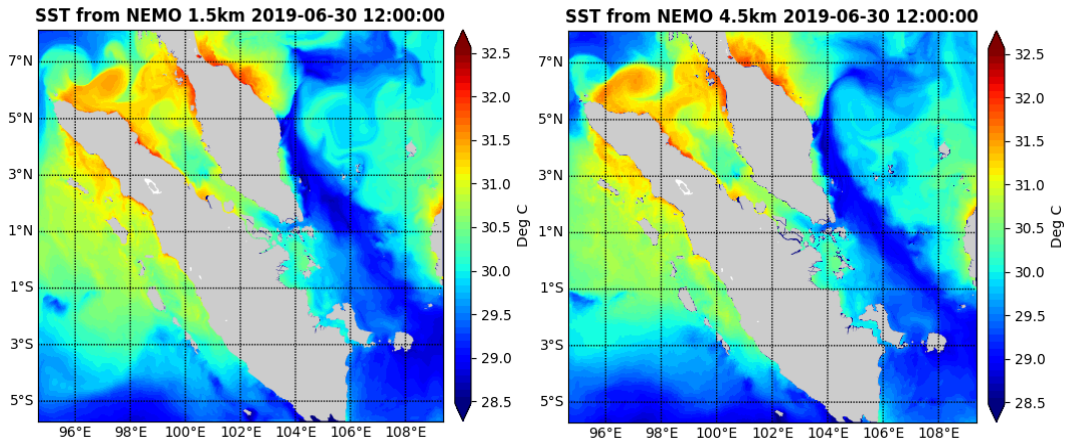

Figure S2. Comparison of the 1.5 km NEMO configuration with the prototype 4.5 km NEMO configuration (Thompson et al., 2021).

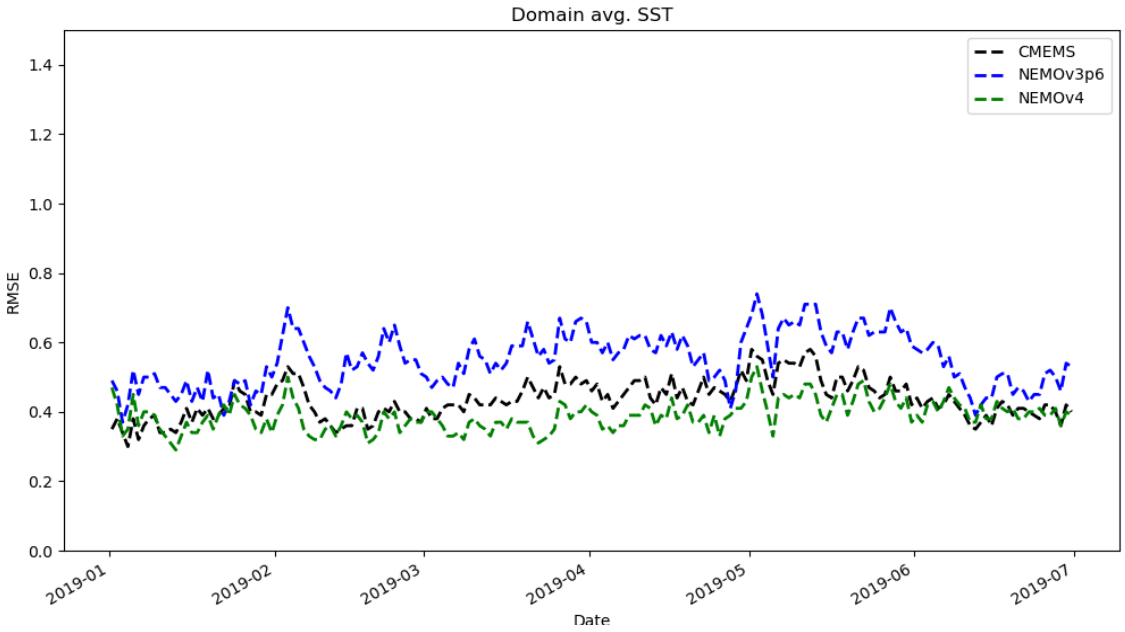

Figure S3. Time series comparison of domain-averaged SST for the 1.5 km (green dashed line) and 4.5 km (blue dashed line) NEMO configurations.

S3. Wave model evaluation and sensitivity

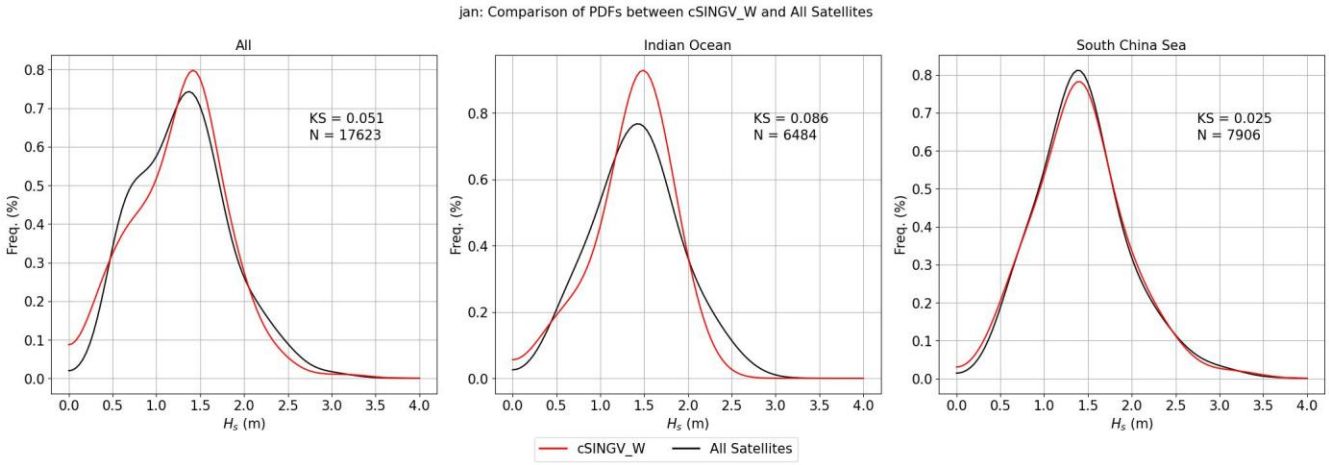

Figure S4. Probability density function (PDF) of significant wave height (Hs) for the cSINGV_W simulation compared with satellite altimeter observations for January 2019.

Table S1. Summary of WAVEWATCH III compilation switches used in the cSINGV_W configuration. Descriptions of key physical parameterisations and numerical options applied in the wave model setup.

Switch	**Summary description**
ST4	Source term package for wave growth & dissipation (Ardhuin et al. 2010)
SMC	Activate SMC grid
FLX0	No separate flux routine; fluxes computed within source terms
LN1	Linear wave growth at low wind speeds (Cavaleri & Rizzoli 1981)
NL1	Discrete interaction approximation (DIA; Hasselmann et al. 1985)
BT1	JONSWAP bottom friction formulation (Hasselmann et al. 1973)
DB1	Depth-induced breaking (Battjes & Janssen 1978)
PR2	Higher-order dispersion correction via the classical GSE alleviation method
UNO	Second-order UNO propagation scheme
WNT1	Linear interpolation of wind over time
WNX1	Approximate linear interpolation of wind over space
RWND	Correct wind speed for current velocity
CRT1	Linear interpolation of current over time
CRX1	Approximate linear interpolation of current over space
SHRD	Shared memory model
NOGRB	No GRIB package included

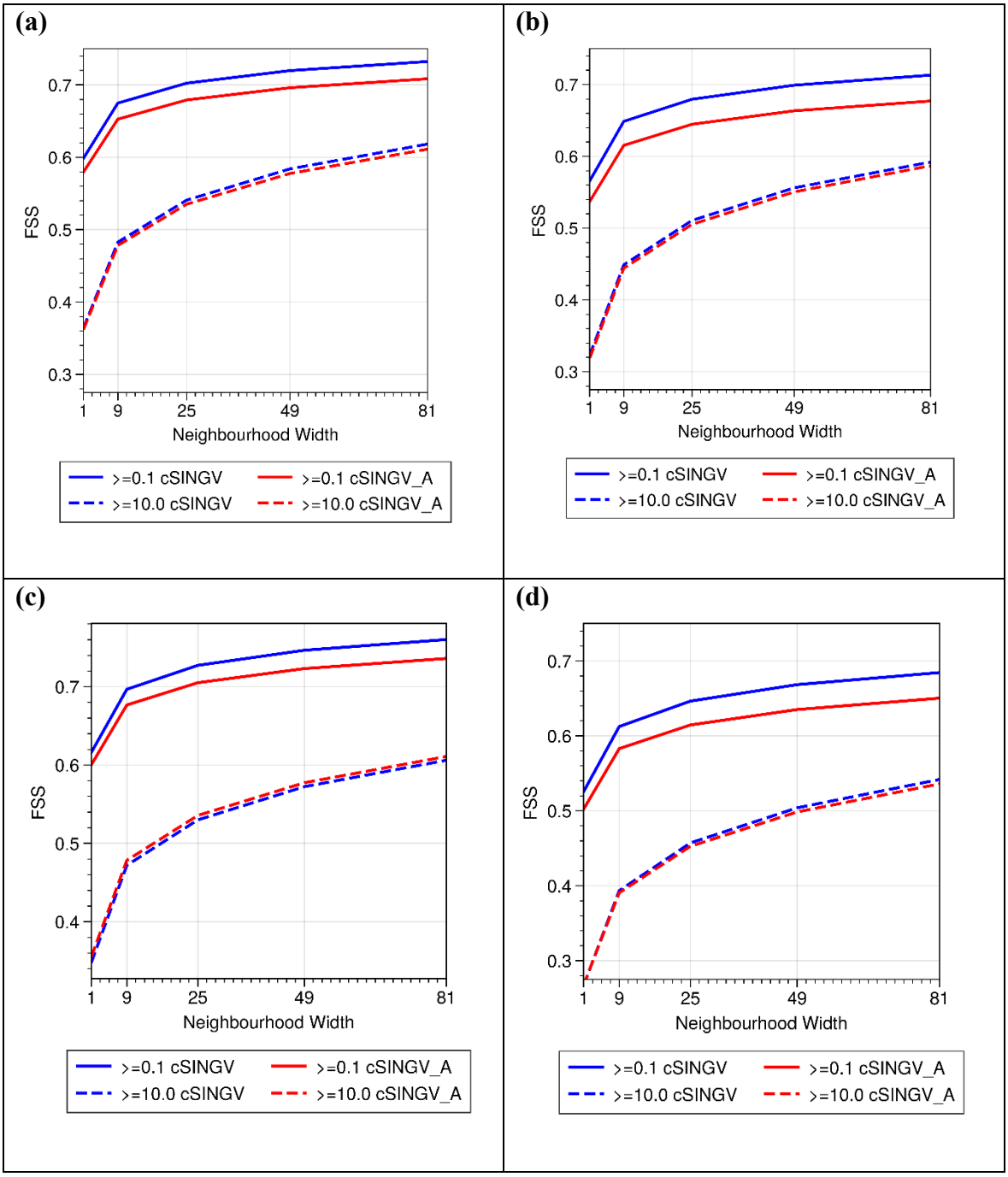

Figure S5. FSS as a function of neighbourhood width for (a) January, (b) February, (c) April, and (d) May 2019, evaluated at two precipitation thresholds: ≥0.1 mm (solid lines) and ≥10.0 mm (dashed lines). Blue lines represent the coupled model (cSINGV) simulations, while red lines represent the uncoupled model (cSINGV_A) simulations. The neighbourhood width is expressed in terms of grid cells; for example, a width of 81 corresponds to a 9 × 9 grid box, equivalent to approximately 13.5 km × 13.5 km at the model resolution of 1.5 km.

S4. Analysis setup and observational datasets

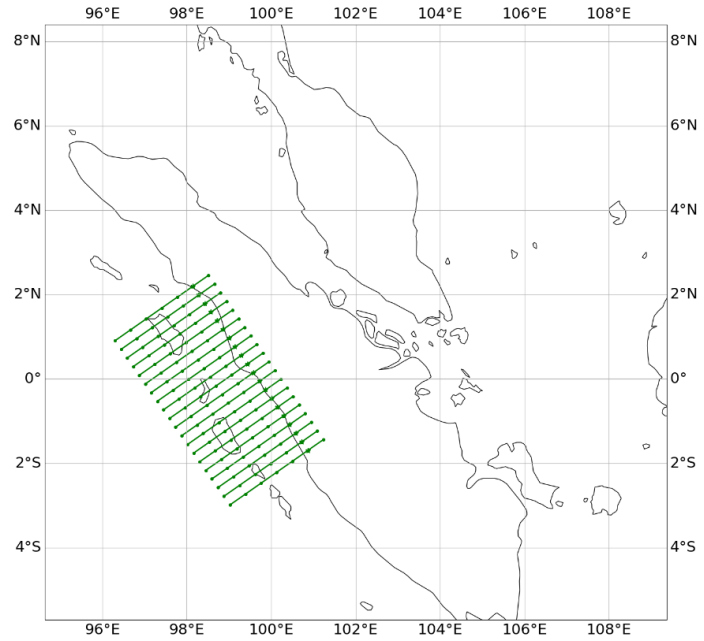

Figure S6. Location and orientation of the transects used for the Hovmöller analysis across western Sumatra. The green lines indicate a set of parallel transects oriented approximately perpendicular to the western coastline of Sumatra, extending from the Indian Ocean (offshore) toward inland regions. These transects are used to construct the diurnal rainfall Hovmöller diagrams shown in Fig. 8.

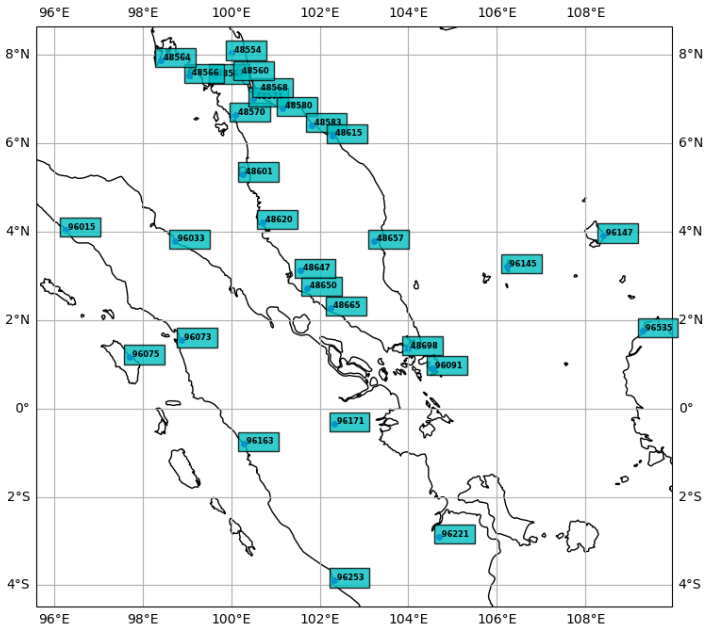

Figure S7. Location of WMO MetDB observation stations used for evaluation. Station IDs correspond to those used in the comparison of near-surface atmospheric variables.

S5. Additional case studies of Sumatra squalls

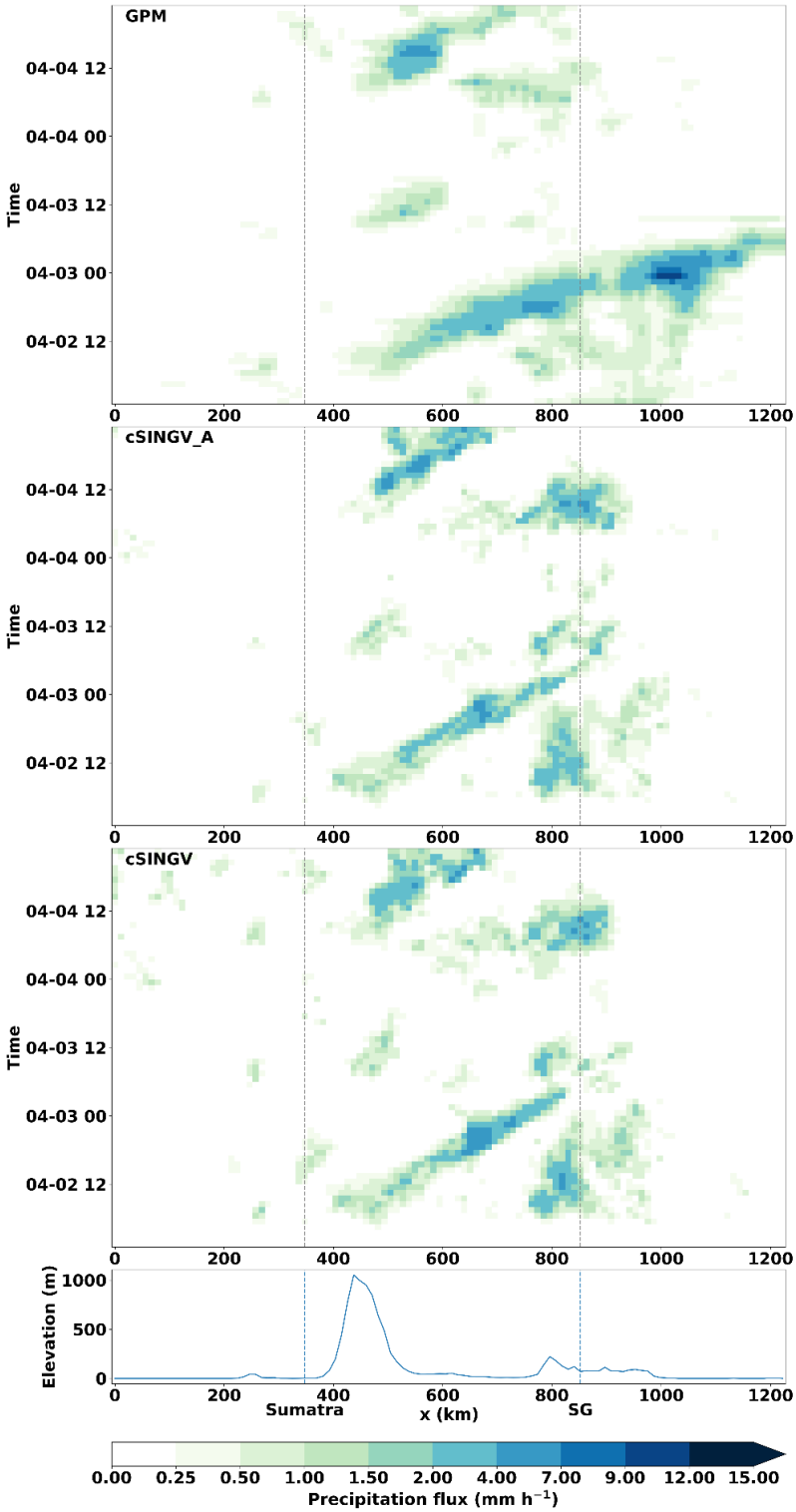

Figure S8. Rotated Hovmöller diagram of precipitation for the 2–4 April 2019 Sumatra squall event. Top: GPM observations; middle: uncoupled simulation (cSINGV_A); bottom: coupled simulation (cSINGV). This case represents a predominantly land-driven convective system.

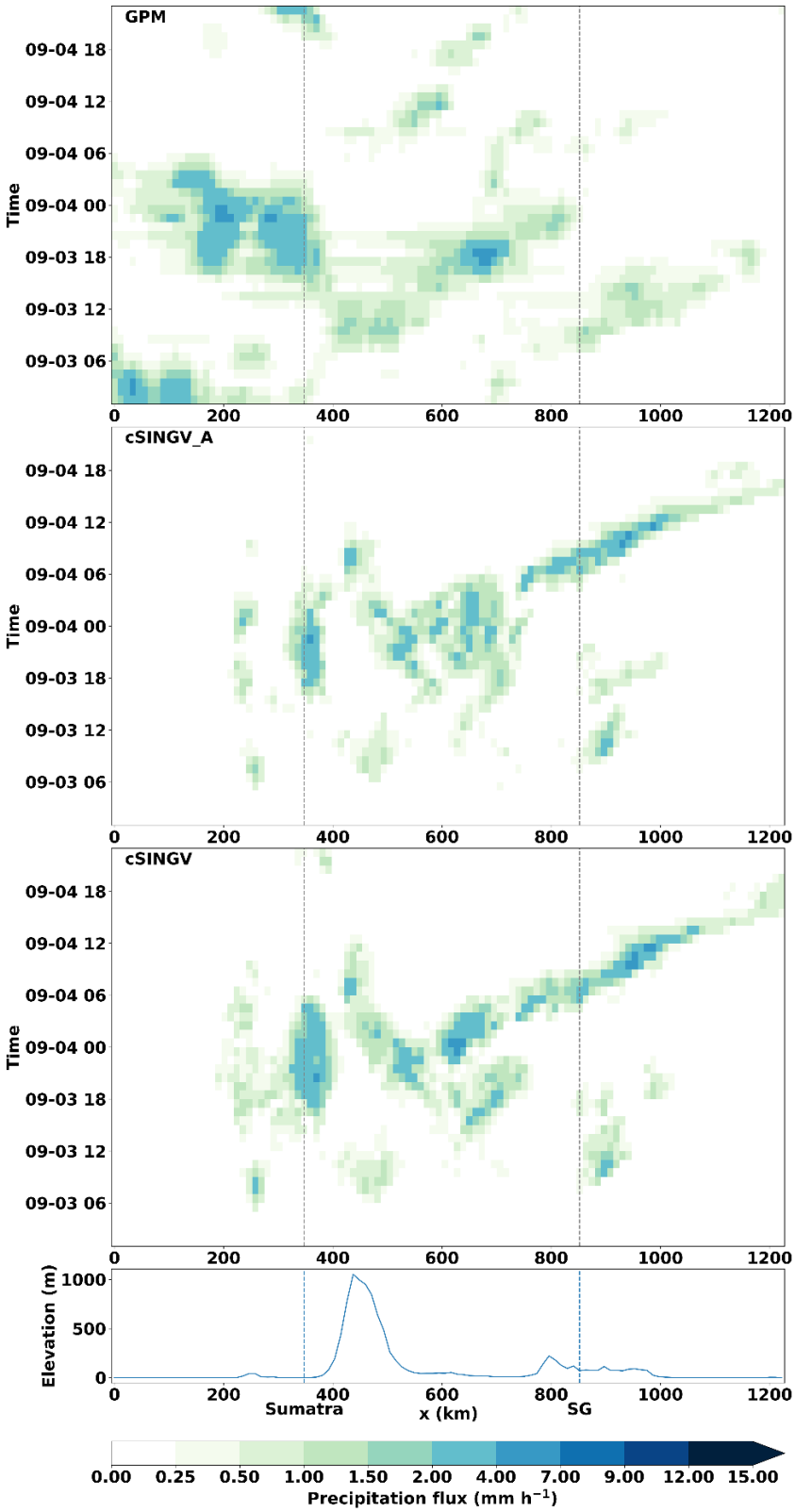

Figure S9. Same as Fig. S8, but for the 3–4 September 2019 event.
The convection exhibits a more fragmented structure during its propagation, with similar behaviour in both configurations.

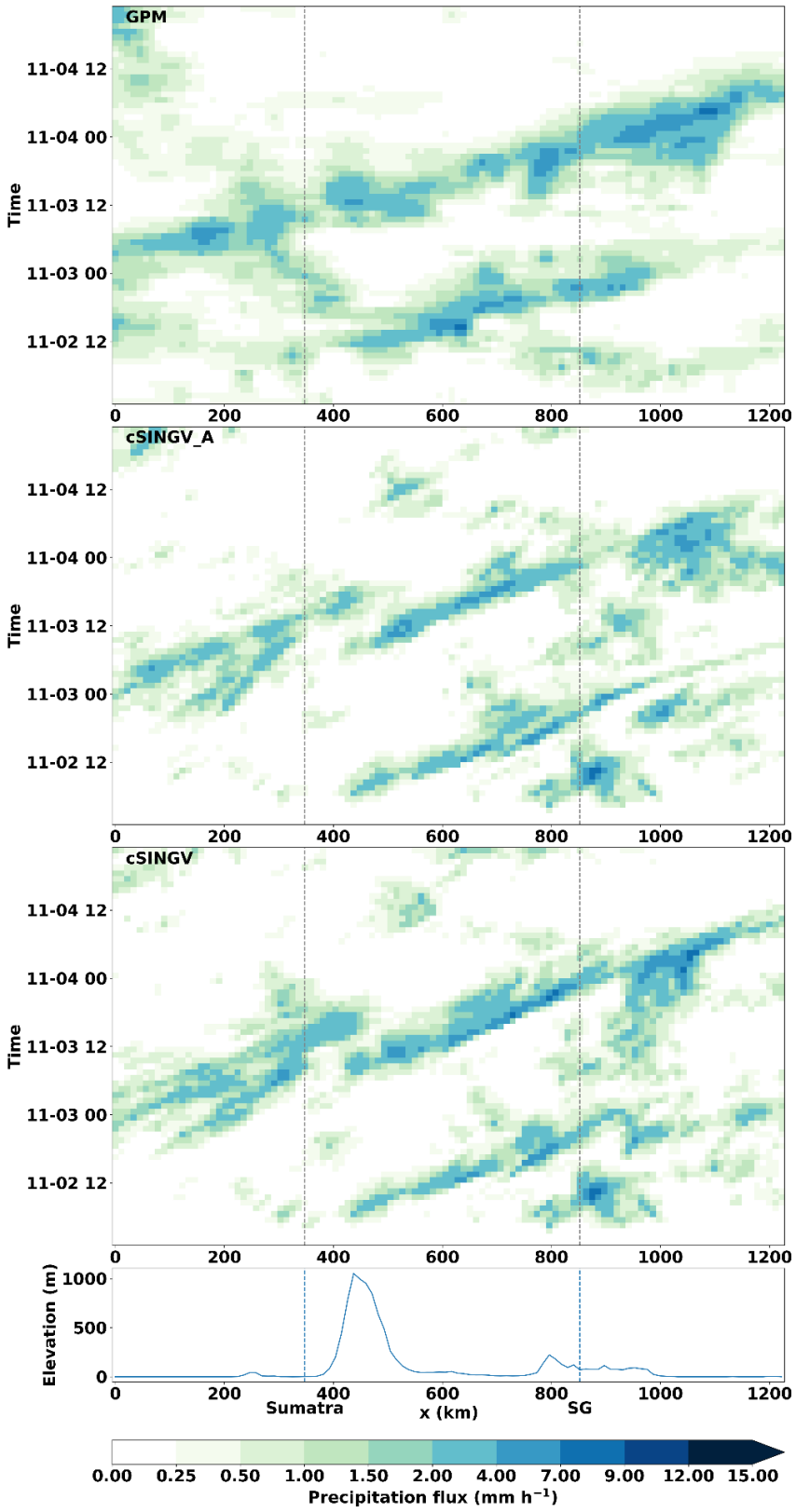

Figure S10. Same as Fig. S8, but for the 2–4 November 2020 event.
This event shows more organised convection and propagation, with the coupled configuration maintaining a more coherent convective structure.

S6. Air–sea flux analysis

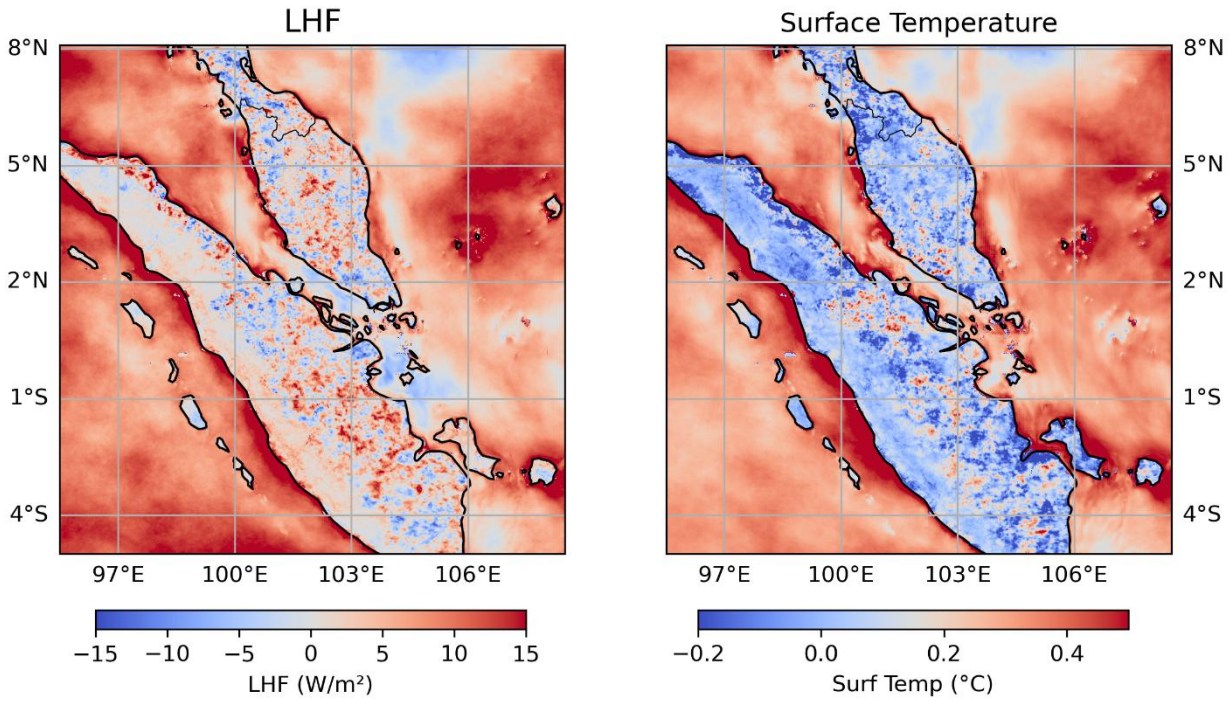

Figure S11. Six-month mean difference (coupled minus uncoupled) in latent heat flux (left) and sea surface temperature (right).

Enhanced upward latent heat flux in the coupled configuration is closely associated with SST differences, highlighting the role of thermodynamic air–sea feedbacks.

S7. Ocean model configuration details

Table S2. Summary of namelist configuration changes applied in the upgrade from NEMO v3.6 to v4.0.4.

Key parameter changes associated with boundary conditions, mixing schemes, advection, and surface forcing are listed.

Namelist	NEMO v4.0.4	NEMO v3.6
nambbl	nn_bbl_ldf=1 rn_ahtbbl=1000. rn_gambbl=10.	nn_bbl_ldf=0
nambdy	ln_bdy=.true. rn_time_dmp=1. rn_time_dmp_out=1	ln_sponge=.true. rn_sponge=5
namdom	?	?
namdyn_ldf	ln_dynldf_blp=.true. ln_dynldf_lev=.true. nn_ahm_ijk_t=31 rn_ahm_b=0. rn_csmc=3.5	ln_dynldf_bilap=.true. ln_dynldf_level=.true. rn_ahm_0_blp=-6.0e7 rn_ahm_m_blp=-6.0e7 rn_cmsh=1

	rn_minfac=1.0 rn_maxfac=1.0	rn_cmsmag_1=3.0 rn_cmsmag_2=3
		[namelist:namdyn_nept] ln_neptramp=.true. rn_htrmax=200.0 rn_htrmin=100.0 rn_tslse=1.2e4 rn_tslsp=3.0e3
nameos	ln_eos80=.true. rn_a0=1.6550e-1 rn_b0=7.6554e-1 rn_lambda1=5.9520e-2 rn_lambda2=7.4914e-4 rn_lambda2=7.4914e-4 rn_mu1=1.4970e-4 rn_mu2=1.1090e-5 rn_nu=2.4341e-3	
namsbc	ln_traqsr=.true.	
namsbc_blk/ namsbc_core (v3.6)	ln_coare_3p5=.true. rn_zqt=2.	rn_zqt=10
namtra_adv	ln_traadv_fct=.true	ln_traadv_tvd=.true.
namtra_ldf	ln_traldf_blp=.true. ln_traldf_lev=.true.	ln_traldf_lap=.true. ln_traldf_hor=.true.
namdyn_spg	ln_dynspg_ts=.true. ln_bt_av=.true. nn_bt_flt=1 ln_bt_auto=.true. rn_bt_cmax=0.8 nn_baro=10	
namtra_qsr	ln_qsr_rgb=.true. rn_abs=0.58 rn_si1=23.0	ln_traqsr=.true. ln_qsr_rgb=.true. rn_abs=0.56 !!rn_si1=20.0
namtrd	ln_tra_trd=.true.	ln_tra_trd=.false.
namzdf	ln_zdfgls=.true.	ln_zdfevd=.true. rn_avevd=60. rn_avm0=1.2e-6 rn_avt0=1.2e-6
namzdf_gls	rn_emin=1.e-7 rn_epsmin=1.e-12	

	ln_length_lim=.true. rn_clim_galp=0.53 ln_sigpsi=.true. rn_crban=100. rn_charn=100000.0 rn_hsro=0.003 rn_frac_hs=1.3 nn_z0_met=1 nn_bc_surf=0 nn_bc_bot=1 nn_stab_func=2 nn_clos=1	

S7. Wave model tuning details (Appendix A)

Table S3. Summary of cSINGV_W tuning for the wave growth parameter (bmax).

Expt. No.	**BETAMAX**	**Correlation**	**Bias**	**RMSE**	**SI**
1	1.0	0.97	-0.18	0.27	0.20
2	1.25	0.97	-0.14	0.25	0.18
3	1.39 (MO)	0.97	-0.12	0.25	0.18
4	1.43 (ECMWF)	0.97	-0.12	0.25	0.18
5	1.5	0.97	-0.11	0.25	0.18
6	1.75	0.97	-0.08	0.24	0.18
7	2.0	0.96	-0.06	0.25	0.18

Table S4. Summary of cSINGV_W tuning for the shallow water physics.

Expt. No.	**Correlation**	**Bias**	**RMSE**	**SI**
8	0.94	+0.06	0.31	0.23
9	0.97	-0.18	0.27	0.20
10	0.97	-0.08	0.24	0.18
11	0.97	-0.19	0.28	0.20
12	0.97	-0.21	0.29	0.21
13	0.97	-0.19	0.28	0.20